On Orientation and Anisotropy Estimation for Online Fingerprint Authentication

Xudong Jiang, *Member, IEEE*

***Abstract*—Local dominant orientation estimation is one of the most important operations in almost all automatic fingerprint authentication systems. Robust orientation and anisotropy estimation improves the system's reliability in handling low-quality fingerprints, which is crucial for the system's massive application such as securing multimedia. This paper analyzes the robustness of the orientation and anisotropy estimation methods and the effect of the modulus normalization on the estimation performance. A two-stage averaging framework with block-wise modulus handling is introduced to inherit the merits of the both linear and normalized averaging methods. We further propose to set the modulus of an orientation vector to be its anisotropy estimate instead of unity so that the orientation inconsistency of gradients is included in the second stage of averaging. These two measures improve the robustness of the fingerprint local dominant orientation estimation and lead to an anisotropy estimate that reflects the characteristics of fingerprint more effectively. In addition, the proposed approach is computationally efficient for online fingerprint authentication. Extensive experiments using both synthetic images and real fingerprints verify the feasibility of the proposed approach and demonstrate its robustness to noise and low-quality fingerprints.**

***Index Terms*—Anisotropy estimation, biometrics, dominant orientation estimation, feature extraction, fingerprint authentication, gradient, image analysis, noise robustness, orientation vector, pattern recognition.**

I. Introduction

BIOMETRIC personal authentication that exploits users' unique physiological characteristics provides a secure solution to protect intellectual property right such as multimedia contents [1]. Fingerprint is the most widely used biometric feature because of the well-known distinctiveness (individuality) and persistence properties of fingerprints over time [2]. To apply fingerprint authentication techniques for the protection of media contents that are to be distributed to massive users, we need to increase the applicability of the authentication system. Because a human's finger is exposed to the outside environment of daily life, a fingerprint sensor may not be able to cope with some extreme skin conditions such as extremely dry and moist skin; therefore, a fingerprint authentication system will unavoidably encounter a certain amount of low-quality fingerprints. A large number of applications, such as securing multimedia, require the system to be robust to low-quality fingerprints.

Manuscript received June 24, 2004; revised October 10, 2004. The associate editor coordinating the review of this manuscript and approving it for publication was Guest Editor Anil K. Jain.

The author is with the School of Electrical and Electronic Engineering, Nanyang Technological University, Singapore 639798 (e-mail: exdjiang@ntu.edu.sg).

Digital Object Identifier 10.1109/TSP.2005.855417

As fingerprint is essentially an oriented texture; its most important intrinsic characteristics are local dominant orientation and anisotropy. They are of great importance in contextual filter design [3], [4] for the optimal image enhancement and feature extraction [5]. Furthermore, local dominant orientation itself is an important feature for fingerprint classification [6], [7], alignment, and matching [8]. Anisotropy is another important measurement for multiscale fingerprint processing [9], fingerprint segmentation [10], [11], and image quality assessment [12]. It is also often used for automatic finger detection and invalid fingerprint rejection in the practical online systems. In recent years, a large number of fingerprint authentication systems have been developed. Although different techniques were employed in different systems, most techniques heavily rely on the orientation and anisotropy estimates (from fingerprint acquisition, image enhancement, parameter estimation and feature extraction to fingerprint alignment, classification, and matching). As a result, robust orientation and anisotropy estimation plays a very important key role in the reliability improvement of an automatic fingerprint authentication system.

There are quite a lot of approaches to estimate the local dominant orientations of an image. A well-developed and most widely used approach is based on averaging squared gradients or principal component analysis of the gradient covariance matrix. It was introduced in [13] and [14] and was widely adopted by a large number of researchers for edge, corner, and line detection [15]–[17], texture analysis [18], [19], and optical flow [20]. Most automatic fingerprint recognition systems employ this gradient-based approach [3], [5], [9], [10], [21]–[24]. This prevalent estimation method consists of two components: gradient computation and squared-gradient averaging. While the gradient captures the orientation information of each individual pixel, the averaging process smooths out noise contained in the gradient and, therefore, extracts the dominant orientation in the neighborhood. This method also introduces an estimate of the image local anisotropy or coherence, which indicates how well the gradients in the neighborhood are pointing in the same direction.

Since this approach averages the squared gradient vectors, the stronger gradients have higher votes in the average orientation than the weaker ones. It was argued that the modulus of the gradient vector should be normalized since we are purely interested in the orientation, and the modulus only reflects the image contrast. Hence, gradient vectors were normalized in the orientation diffusion proposed in [25]. Some approaches for regularizing or smoothing the fingerprint orientation field [3], [24] equivalently average block orientation vectors with normalized moduli. Generally speaking, the linear average is optimal only

to smooth out Gaussian additive noise. A fingerprint is often corrupted by non-Gaussian exclusive or impulsive-like noise. Some nonlinear methods are expected to perform better noise attenuation. Modulus normalization is a simple nonlinear method and is therefore suitable for the online system. However, its effect on noise attenuation needs to be thoroughly studied. Intuitively, modulus normalization can either suppress or amplify noise, depending on the type and level of the oriented pattern and noise. It is therefore of interest to investigate how to handle the modulus of an orientation vector for effective noise attenuation. Another interesting task is to explore the effectiveness of the anisotropy estimate in representing the fingerprint characteristics.

In this paper, we analyze the robustness of the gradient-based orientation and anisotropy estimation methods, as well as the effect of the modulus normalization of gradients on estimation performance. Based on the analysis, a two-stage averaging framework with block-wise modulus handling is introduced to inherit the merits of the both linear and normalized averaging methods in noise attenuation. Furthermore, we propose to set the modulus of an orientation vector to be its anisotropy estimate instead of unity so that the orientation inconsistency of the gradients is included in the second stage of averaging. These two measures enhance the noise robustness of the fingerprint local dominant orientation estimation. In addition, the proposed approach leads to an improved anisotropy estimate that is a useful feature for fingerprint segmentation and quality assessment. Extensive experiments using both synthetic images and real fingerprints verify the feasibility of the proposed approach and demonstrate its superiority to other conventional gradient-based orientation estimation approaches.

II. Gradient-Based Orientation Estimation

A gradient-based method to estimate the local dominant orientations of an image was introduced in [13] and [14] and widely adopted by a large number of researchers for edge, corner, and line detection [16], [17], [26], texture analysis [18], [19], optical flow [20], and fingerprint recognition [3], [5], [9], [10], [21]–[24]. This method can be elegantly described by the principal component analysis (PCA) of the gradient covariance matrix.

A. Orientation and Anisotropy Estimation by PCA

Let $f(x,y)$ be a bandlimited image that is differentiable everywhere. The gradient image is given by $\nabla f(x,y) = [f_x(x,y),\ f_y(x,y)]$, where $f_x(x,y)$ and $f_y(x,y)$ are the x- and y-differentials of image $f(x,y)$, respectively. The gradient covariance matrix of a region Γ is computed by

$$C^{\Gamma} = \begin{bmatrix} S^{\Gamma}_{xx} & S^{\Gamma}_{xy} \\ S^{\Gamma}_{xy} & S^{\Gamma}_{yy} \end{bmatrix} = \frac{1}{N}\sum_{\Gamma} \nabla f(x,y)^T \nabla f(x,y) \qquad (1)$$

where N is the number of gradients in the estimation region Γ.

If the eigenvectors V_1 and V_2 of the gradient covariance matrix C^{Γ} have their corresponding eigenvalues λ_1 and λ_2 with $\lambda_1 > \lambda_2$, the dominant orientation of the image in the local estimation region Γ is the orientation of the eigenvector V_2, and the anisotropy estimate is given by

$$Q^{\Gamma} = \frac{\lambda_1 - \lambda_2}{\lambda_1 + \lambda_2}. \qquad (2)$$

B. Averaging Under Polar Coordinate System

The above principal component analysis (PCA) of the gradient covariance matrix provides exactly the same results as the squared-gradient averaging method for the local dominant orientation and anisotropy estimation [23]. To facilitate the discussion of its noise robustness and the effect of the gradient modulus normalization on the estimation performance, we will express the squared-gradient averaging method under polar coordinate system. This also helps us to conduct our proposed approach, which improves noise robustness. For the symbolic simplicity, we replace the pixel index (x,y) with (t).

Let us represent the gradient by a complex variable as $\nabla f(t) = f_x(t) + jf_y(t)$. The squared gradient can be, under the polar coordinate system, expressed as

$$r(t)e^{j\varphi(t)} = f_x^2(t) - f_y^2(t) + 2jf_x(t)f_y(t) \qquad (3)$$

with the modulus and angle calculated by

$$\begin{aligned} r(t) &= \sqrt{\left(f_x^2(t) - f_y^2(t)\right)^2 + 4(f_x(t)f_y(t))^2} \\ &= f_x^2(t) + f_y^2(t) \qquad (4) \\ \varphi(t) &= \angle\left[f_x^2(t) - f_y^2(t), 2f_x(t)f_y(t)\right]. \qquad (5) \end{aligned}$$

The average squared-gradient in the region Γ can be expressed as

$$R^{\Gamma}e^{j\phi^{\Gamma}} = \frac{1}{N}\sum_{\Gamma} r(t)e^{j\varphi(t)}. \qquad (6)$$

The modulus and angle of the average squared-gradient vector can be computed as

$$\begin{aligned} R^{\Gamma} &= \sqrt{\left(S^{\Gamma}_{xx} - S^{\Gamma}_{yy}\right)^2 + 4\left(S^{\Gamma}_{xy}\right)^2} \qquad (7) \\ \phi^{\Gamma} &= \angle\left[S^{\Gamma}_{xx} - S^{\Gamma}_{yy}, 2S^{\Gamma}_{xy}\right] \qquad (8) \end{aligned}$$

where S^{Γ}_{xx}, S^{Γ}_{yy}, and S^{Γ}_{xy} are computed by (1).

The estimated local dominant orientation of the region Γ is perpendicular to $\phi^{\Gamma}/2$, which is the same as the angle of the eigenvector of C^{Γ}, which corresponds to the smaller eigenvalue. It is not difficult to obtain the anisotropy estimate as

$$Q^{\Gamma} = \frac{R^{\Gamma}}{\frac{1}{N}\sum_{\Gamma} r(t)}. \qquad (9)$$

We see from (9) that the anisotropy estimate is measured by the modulus of the average squared-gradient divided by the average modulus of the squared gradients. If all gradients are pointing in exactly the same direction, Q^{Γ} reaches 1. The uniform distribution of gradients in all orientations or in orthogonal orientations results in a Q^{Γ} value of 0.

From (6), both the modulus and the angle of the squared gradient are incorporated in the averaging that will affect the estimation result. The stronger gradients have higher votes in the

averaging process than the weaker ones. The argument is then if we should normalize the gradient modulus before averaging (6). Although the anisotropy estimate (9) is normalized to $[0, 1]$ by the average modulus of gradients in the estimation region, the stronger gradients within the estimation region Γ still have higher votes in the anisotropy estimate than the weaker ones. Therefore, it is of great interest to explore the characteristics of the orientation and anisotropy estimates with and without modulus normalization.

III. Robust Estimation by Modulus Handling

A. Noise-Corrupted Gradient Image Modeling

We model the noise corrupted image as

$$f(t) = \begin{cases} c(t)s(t) + n(t), & \text{with prob. } p \\ m(t), & \text{with prob. } 1-p \end{cases} \tag{10}$$

where $s(t)$ is the oriented pattern (signal), and $n(t)$ and $m(t)$ are additive and exclusive (or called impulsive) noise, respectively. The nonconstant variable $c(t)$ reflects the image contrast inconsistency. Fig. 1 shows a portion of a real fingerprint. If the signal pattern is modeled by the white and black lines in Fig. 1, there is noise $n(t)$ added to most pixels of ridges and noise $m(t)$ (the ridge break) replacing the signal pattern. The varying contrast $c(t)$ is also shown in Fig. 1.

From (10), the gradient image can be expressed as

$$\nabla f(t) = \begin{cases} c(t)\nabla s(t) + \nabla n(t), & \text{with prob. } p \\ \nabla m(t), & \text{with prob. } 1-p. \end{cases} \tag{11}$$

We ignore the item of the derivative of $c(t)$ in (11) since it is usually very small due to the slow change of $c(t)$.

In most practical fingerprint images, not every pixel is added by noise $n(t)$, or the additive noise of some pixels are so small that it can be ignored. The fingerprint signal pattern $s(t)$ usually produces strong gradients on the edges between ridges and valleys and almost zero gradients within them, especially for images obtained by solid-state (silicon) sensors, where $s(t)$ can be modeled by the white and black lines with corresponding constant gray levels. Gradients within ridges and valleys are therefore contributed mainly by noise, and noise $n(t)$ usually gives an ignorable contribution to gradients on the edges between the ridges and valleys. For a signal pattern $s(t)$ that has sinusoidal shape, the modulus of its gradient varies periodically between the maximum and zero. Gradients are thus usually contributed by the signal or the exclusive noise $m(t)$ near the ridge-valley edges and by noise $n(t)$ and $m(t)$ within ridges and valleys. Therefore, we can separate the gradients of additive noise $\nabla n(t)$ from the the signal gradients for most practical fingerprint images. The squared gradient image can be modeled as

$$r(t)e^{j\varphi(t)} = \begin{cases} d(t)r_s(t)e^{j\varphi_s(t)}, & \text{with prob. } p' \\ r_n(t)e^{j\varphi_n(t)}, & \text{with prob. } p-p' \\ r_m(t)e^{j\varphi_m(t)}, & \text{with prob. } 1-p \end{cases} \tag{12}$$

where $d(t) = c^2(t)$, and $r_s(t)$, $r_n(t)$, and $r_m(t)$ are the squared gradient amplitudes of $s(t)$, $n(t)$, and $m(t)$, respectively. p' is the probability of the significant gradient of $s(t)$ and $p' \le p$. If $s(t)$ is a pattern of white and black lines, p' is the probability of the nonzero gradient of $s(t)$.

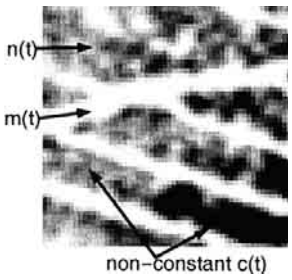

Fig. 1. Portion of real fingerprint showing additive noise $n(t)$, exclusive noise $m(t)$, and the nonconstant contrast $c(t)$.

B. Problems of Linear and Normalized Averages

To explore problems of linearly averaging the squared gradients and study the pros and cons of the gradient modulus normalization, we change the squared gradient average (6) into a more general weighted average and partition the sum into three items according to (12) as

$$R_w^\Gamma e^{j\phi_w^\Gamma} = \frac{1}{N}\left(\sum_{\Omega_s} w(t)d(t)r_s(t)e^{j\varphi_s(t)} + \sum_{\Omega_n} w(t)r_n(t)e^{j\varphi_n(t)} + \sum_{\Omega_m} w(t)r_m(t)e^{j\varphi_m(t)}\right) \tag{13}$$

where $\Omega_s \cup \Omega_n \cup \Omega_m = \Gamma$. The orientation estimate is

$$\Theta_w^\Gamma = \frac{\phi_w^\Gamma}{2} + \frac{\pi}{2} \tag{14}$$

and the anisotropy estimate is given by

$$Q_w^\Gamma = \frac{R_w^\Gamma}{\frac{1}{N}\sum_\Gamma w(t)r(t)}. \tag{15}$$

From (13)–(15), the orientation and anisotropy estimates with the linear average denoted by Θ_1^Γ and Q_1^Γ are obtained by $R_1^\Gamma e^{j\phi_1^\Gamma}$ with $w(t) = 1$, and those with the gradient-normalized average denoted by Θ_r^Γ and Q_r^Γ are obtained by $R_r^\Gamma e^{j\phi_r^\Gamma}$ with $w(t) = 1/(r(t) + \epsilon)$, where ϵ is the smallest positive floating-point number in the computer to handle the $0/0$ condition. Generally speaking, normalization of the gradient modulus suppresses the larger gradients and amplifies the smaller ones.

For the oriented texture such as the fingerprint, the important information is contained in the orientation, rather than in the brightness and contrast values. More generally, the fingerprint image consists of ridge- and valley-curves rather than straight lines in the estimation region. This results in $\varphi_s(t)$ not being a constant in the estimation region Γ. The desired dominant orientation estimate should capture the orientation of the curve at the center of the region Γ or some kind of mean of the "signal" orientation distribution (*note*: not the mean of the orientation vectors). The varying $r_s(t)$ does not affect the orientation estimation much as $r_s(t)$ varies periodically, and the estimation region Γ usually captures four to six periods of $r_s(t)$ (two to three ridge/valley periods). However, the nonconstant value of $d(t)$ in (13) may result in an estimate Θ_1^Γ that deviates from the desired orientation. In this case, modulus normalization will produce a more accurate or more reasonable orientation estimate Θ_r^Γ. Fig. 2(a) shows a noise-free oriented

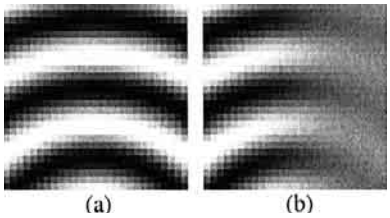

Fig. 2. Curvy oriented patterns with (a) constant and (b) varying contrasts.

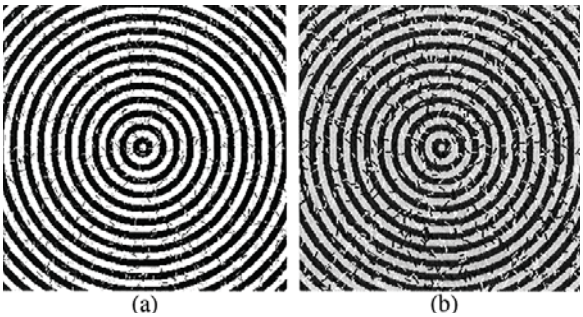

Fig. 3. Two sample-oriented patterns with 10% of the pixels corrupted by noise with gray level (a) half and (b) double of that of the "signal" pattern.

pattern of size 27×27 pixels with $n(t) = 0$, $p = 1$, and $c(t) = 1$. The signal pattern is a portion of a sinusoidal circle $s(t) = \sin(0.2\pi\sqrt{x^2 + (y+27)^2})$ with $t = (0,0)$ at the image center point. The desired orientation is 0°. Indeed, the orientation estimation with (13) and (14) produces $\Theta_1^\Gamma = 0°$ and $\Theta_r^\Gamma = 0°$. Note that in all tests of computing the orientation estimate in this paper, we use a 3×3 Sobel operator to produce the gradient and set $\Gamma = 25 \times 25$. If we add a varying contrast $c(t) = \tanh(-0.35x) + 1.3$ in the estimation region, as shown in Fig. 2(b), the orientation estimation with (13) and (14) leads to $\Theta_1^\Gamma = 13.4574°$ and $\Theta_r^\Gamma = 0.7690°$. This example clearly shows the benefit of the modulus normalization in solving the contrast inconsistency problem.

It is well known that the sum of two vectors points to an orientation closer to the vector with a larger modulus than the one with a smaller modulus. Based on the noise gradient model (12) and the squared gradient average model (13), if noise gradients are weaker than those of the signal, the normalized average amplifies noise gradients and, therefore, results in a larger estimation error than the linear average. However, the orientation estimation will benefit from the normalization if noise gradients are stronger than those of the signal. Fig. 3(a) and (b) show two samples of oriented image of size 252×252 with 10% of the pixels corrupted by exclusive oriented noise $m(t)$, $1 - p = 0.1$, $n(t) = 0$, and $c(t) = 1$. The signal pattern $s(t)$ consists of alternate circle ridges and valleys of width 6 with respect to the constant gray levels. Noise is simulated by random oriented lines that are 1 pixel in width and 5 pixels in length. The image is divided into 100 nonoverlapping local estimation regions. For the noise-free pattern ($p = 1$), Θ_1^Γ and Θ_r^Γ achieve the average absolute errors of 1.0714° and 2.1871°, respectively. We see that the linear average results in smaller estimation bias than the normalized average. We generate 20 noisy image samples ($1 - p = 0.1$) with independent random noise and estimate their

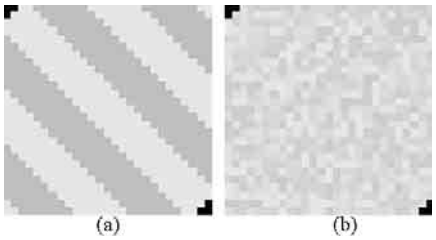

Fig. 4. Two 27×27 image blocks where six noise pixels with a gray value of 0 are injected in (a) a noise-free oriented pattern with gray level 223/255 and (b) a noise pattern with gray level uniformly distributed in $[235\ 255]$.

local dominant orientations of all estimation regions (2000 estimates altogether). By setting the noise gray level, half of the signals, as shown in the sample image Fig. 3(a), Θ_1^Γ, and Θ_r^Γ, result in the average absolute errors of 1.4023° and 2.2521°, respectively. However, by setting the noise gray level to twice the signal's, as shown in the sample image Fig. 3(b), they increase to 3.3551° and 2.7686°, respectively. This example clearly shows the pros and cons of the modulus normalization.

To study the effect of modulus normalization on the anisotropy estimate, we first see the anisotropy estimation results of the two examples in Fig. 2. The anisotropy estimates computed by (13) and (15) are $Q_1^\Gamma = 0.8501$ and $Q_r^\Gamma = 0.8488$ for Fig. 2(a). No remarkable difference is seen. A smaller anisotropy estimate is expected to reflect the lower quality of Fig. 2(a) than Fig. (b). This is true in the case of normalization (Q_r^Γ decreases to 0.6451) but not true in the case of linear average. (Q_1^Γ increases to 0.9139.) Indeed, Q_1^Γ may have a serious problem in some cases as the stronger gradients have higher votes in the average. Fig. 4(a) shows an oriented pattern of size $27 \times 27 = 729$ pixels, where only six pixels (less than 1%) are corrupted by strong noise. If these six pixels are not corrupted, we have $Q_1^\Gamma = Q_r^\Gamma = 1$. If the six corrupted pixels have a gray level of zero and the ridge and valley of the oriented pattern have the gray levels of 223 and 255, respectively, as shown in Fig. 4(a), Q_1^Γ sharply decreases to 0.1117. On the other hand, a random noise pattern with the pixel gray level uniformly distributed between 235 and 255 plus six impulsive pixels of gray level of zero, as shown in Fig. 4(b), achieves a very high anisotropy estimate $Q_1^\Gamma = 0.8643$. This shows a serious defect of Q_1^Γ in the anisotropy measurement of a fingerprint where the information we want to capture should be represented by the majority of pixels rather than that represented by a few pixels with strong contrast. Gradient normalization leads to a much better anisotropy estimate with $Q_r^\Gamma = 0.9667/0.0676$ for Fig. 4(a) and (b).

These two examples show that the anisotropy estimate with a normalized average reflects the characteristics of the oriented texture much better than that of linear average. However, this is not quite true for the oriented patterns in Fig. 3. The average values of Q_1^Γ and Q_r^Γ over the 2000 image blocks are 0.7692 and 0.5155 for Fig. 3(a) and 0.5035 and 0.4596 for Fig. 3(b), respectively. Both Fig. 3(a) and (b) have the same signal and noise patterns, but the noise level of Fig. 3(b) is four times higher than that of Fig. 3(a). The anisotropy estimate Q_1^Γ reflects this difference of image quality with the anisotropy difference of 0.2657 much better than Q_r^Γ with the anisotropy difference of

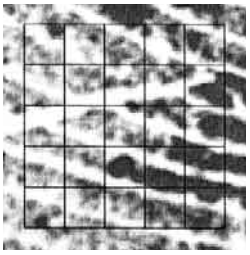

Fig. 5. Partial real fingerprint, the estimation region Γ (the largest square), and the 25 blocks Λ_k (the smallest squares).

only 0.0559. Note that both Q_1^Γ and Q_r^Γ have the same maximum and minimum values of 1 and 0.

C. Proposed Two-Stage Estimation Framework

We studied the problems and defects of the both linear and gradient-normalized averaging methods in the local dominant orientation and anisotropy estimation. To find the solution of these problems, we first explore an estimation region Γ of a typical real fingerprint image, as shown in Fig. 5. We partition the estimation region Γ into small blocks Λ_k, where each block is supposed to capture at least a half period of fingerprint ridge and valley structure (Λ_k is supposed to cover at least a period of $r_s(t)$), as shown in Fig. 5. The size of Λ_k can be determined by a ridge density estimation algorithm such as [27] or predetermined based on the prevalent fingerprint ridge-valley width.

From Fig. 5, we can see some useful phenomena:

1) Each small block contains a signal pattern, and weak noise is densely distributed in every small block, i.e., a large number of pixels in every small block contains weak noise.
2) Contrast inconsistency $c(t)$ can be ignored within the small blocks, but it can have significantly different values in different blocks.
3) Strong oriented noise such as stroke noise usually sparsely occurs only in a small number of blocks.

Phenomena 1) and 2) teach us that we should linearly average the squared gradients within each block Λ_k to smooth weak noise more effectively. The linear average on Λ_k produces the dominant orientation and anisotropy estimates of block Λ_k. Based on phenomena 2) and 3), we should normalize moduli of the dominant orientation vectors of blocks Λ_k to suppress the possible strong noise and solve the contrast inconsistency problem $c(t)$ before further averaging them over the set Γ^Λ. Set Γ^Λ represents the same geometric window as Γ, whereas its elements are not the pixel indexes t but the block indexes k. Therefore, an improved averaging framework can be formulated as

$$R_{w\Lambda}^\Gamma e^{j\phi_{w\Lambda}^\Gamma} = \frac{1}{N}\sum_{k\in\Gamma^\Lambda} w(k)\sum_{t\in\Lambda_k} r(t)e^{j\varphi(t)}. \tag{16}$$

From (7), the modulus normalization of the orientation vector of block Λ_k is implemented by setting the weights in (16) as

$$w(k) = \frac{1}{R_1^{\Lambda_k}+\epsilon} = \frac{1}{\sqrt{\left(S_{xx}^{\Lambda_k} - S_{yy}^{\Lambda_k}\right)^2 + 4\left(S_{xy}^{\Lambda_k}\right)^2}+\epsilon}. \tag{17}$$

The resulting orientation and anisotropy estimates by (16) and (17) are denoted by $\Theta_{R\Lambda}^\Gamma$ and $Q_{R\Lambda}^\Gamma$, respectively. This average framework consists of two stages: The first one linearly averages gradients within each small block to produce block-dominant orientation vectors $R_1^{\Lambda_k}e^{j\phi_1^{\Lambda_k}}$, and the second one averages the normalized orientation vectors throughout all blocks Λ_k to produce the final dominant orientation vector of the estimation region Γ. Compared with the linear and gradient-normalized averages, this block-wise normalization framework more effectively smooths out mixed weak Gaussian-like and strong impulsive-like noise and solves the contrast inconsistency problem. Keeping in mind that a heavily corrupted image block could be due to the strong (in amplitude) and/or dense (in occurrence) noise in that block, this block-wise normalization can also suppress dense noise in some blocks, whereas gradient normalization can only suppress strong noise of some gradients.

D. Proposed Modulus Handling of the Block Orientation Vector

The modulus normalization of the block orientation vector brings one problem. It ignores the orientation inconsistency of gradients within the block Λ_k by setting the vector moduli of all blocks to unity in (16) for the second stage of the average. A nearly isotropic block caused by heavy noise, regardless of its contrast, produces an orientation vector with a very small modulus. This very small modulus will be greatly amplified by the normalization, which could lead to a larger error of the orientation estimate $\Theta_{R\Lambda}^\Gamma$ than Θ_1^Γ and Θ_r^Γ. In addition, the anisotropy estimate $Q_{R\Lambda}^\Gamma$ reflects only the interblock orientation inconsistency, ignoring the intrablock ones.

Recalling that we average vectors rather than scalars, noise in a block may not only increase the modulus of the orientation vector of that block but also decrease it, depending on the noise levels and orientations relative to those of the signal pattern. In the second stage of the average, smaller $R_1^{\Lambda_k}$ caused by lower contrast or weak or sparse noise should be amplified, but that caused by the inconsistency of gradient orientations within Λ_k should not; for larger $R_1^{\Lambda_k}$ caused by high contrast, strong or dense noise should be suppressed, but that caused by the good consistency of gradient orientations within Λ_k should not. Therefore, instead of normalizing the modulus, we set it to be the block's anisotropy estimate $Q_1^{\Lambda_k}$ for the second stage of average as

$$R_{Q\Lambda}^\Gamma e^{j\phi_{Q\Lambda}^\Gamma} = \frac{1}{M}\sum_{k\in\Gamma^\Lambda} Q_1^{\Lambda_k} e^{j\phi_1^{\Lambda_k}} \tag{18}$$

where M is the number of blocks Λ_k in the estimation region Γ.

From (6) and (9), we have

$$R_1^{\Lambda_k} e^{j\phi_1^{\Lambda_k}} = \frac{1}{L}\sum_{\Lambda_k} r(t)e^{j\varphi(t)} \tag{19}$$

and

$$Q_1^{\Lambda_k} = \frac{R_1^{\Lambda_k}}{\frac{1}{L}\sum_{\Lambda_k} r(t)} \tag{20}$$

1) Compute the gradients $\nabla f(t)$ at all pixels t of a fingerprint (simple Sobel operator is used in our experiments).

2) Divide the fingerprint image into non-overlapping blocks Λ_k (of size 5×5 pixels in our experiments) and compute the gradient covariance matrices of all blocks Λ_k by

$$\begin{bmatrix} S_{xx}^{\Lambda_k} & S_{xy}^{\Lambda_k} \\ S_{xy}^{\Lambda_k} & S_{yy}^{\Lambda_k} \end{bmatrix} = \sum_{t\in\Lambda_k} \nabla f(t)^T \nabla f(t). \tag{22}$$

3) Divide the block field $\{\Lambda_k\}$ into non- or overlapping regions Γ_m (of size 5×5 blocks Λ_k in our experiments) and compute the dominant orientation vectors of all regions Γ_m by

$$R_{Q\Lambda}^{\Gamma_m} e^{j\phi_{Q\Lambda}^{\Gamma_m}} = \sum_{\Lambda_k\in\Gamma_m} \frac{S_{xx}^{\Lambda_k} - S_{yy}^{\Lambda_k} + 2jS_{xy}^{\Lambda_k}}{S_{xx}^{\Lambda_k} + S_{yy}^{\Lambda_k} + \epsilon}. \tag{23}$$

4) The orientation estimates of all regions Γ_m are given by

$$\Theta_{Q\Lambda}^{\Gamma_m} = \phi_{Q\Lambda}^{\Gamma_m}/2 + \pi/2. \tag{24}$$

5) The anisotropy estimates of all regions Γ_m are given by

$$Q_{Q\Lambda}^{\Gamma_m} = R_{Q\Lambda}^{\Gamma_m}/M. \tag{25}$$

Fig. 6. Proposed algorithm for estimating the orientation and anisotropy fields of a fingerprint.

where L is the number of gradients in the block Λ_k. We see that in the second stage of the average, the modulus of an orientation vector is set to be 1 only if all gradients in that block are pointing in exactly the same direction. Orientation inconsistency of the gradients in a block decreases the vector modulus of that block in the second stage of the average. The orientation vector of a block will vanish from the second stage of the average if gradients in that block are distributed evenly in all orientations or equally in orthogonal orientations. In addition, the interblock image contrast change will not affect the orientation estimation.

Substituting (19) and (20) into (18) and comparing the result with (16), setting the modulus of an orientation vector to be its anisotropy estimate $Q_1^{\Lambda_k}$ for the second stage of the average can be realized by setting the weights in the second stage of the average (16) as

$$w(k) = \frac{1}{\frac{1}{L}\sum\limits_{t\in\Lambda_k} r(t) + \epsilon} = \frac{1}{S_{xx}^{\Lambda_k} + S_{yy}^{\Lambda_k} + \epsilon}. \tag{21}$$

Substituting (1), (3), and (21) into (16) and omitting L and M, which have no effect on the estimation, the proposed orientation and anisotropy estimation algorithm for a fingerprint image is summarized in Fig. 6.

The proposed algorithm in Fig. 6 is a single-step process with a predetermined size of the estimation region Γ (25×25 in our experiments). The estimation regions can overlap so that we can have a denser orientation field. As the grid of size 5×5 provides sufficient resolution for fingerprint recognition (16×16 is commonly used in the fingerprint recognition system), we suggest nonoverlapping blocks Λ_k. In the high curvature area near the core and delta points, the estimation region size of 25×25 may be too large to catch the orientation of the region center. In this case, we suggest using the size 3×3 blocks for the second stage of the average. The effective size of the estimation region is reduced to 15×15. On the other hand, a larger estimation region may be needed at the heavily noised fingerprint area. In this case, we suggest applying the proposed algorithm iteratively, which is similar to the orientation regularization [8], [10] and diffusion [25] frameworks. The key issue is to determine the number of the iteration or the size of the estimation region adaptively, which is, however, not a well-solved problem. The commonly used measurements to determine the number of the iteration or the size of the estimation region cannot differentiate the portion caused by noise from the portion caused by curvature: One indicates a larger estimation region, and the other contrarily indicates a smaller one. Therefore, we do not study further the effects of the iterative application of the proposed algorithm before solving this problem.

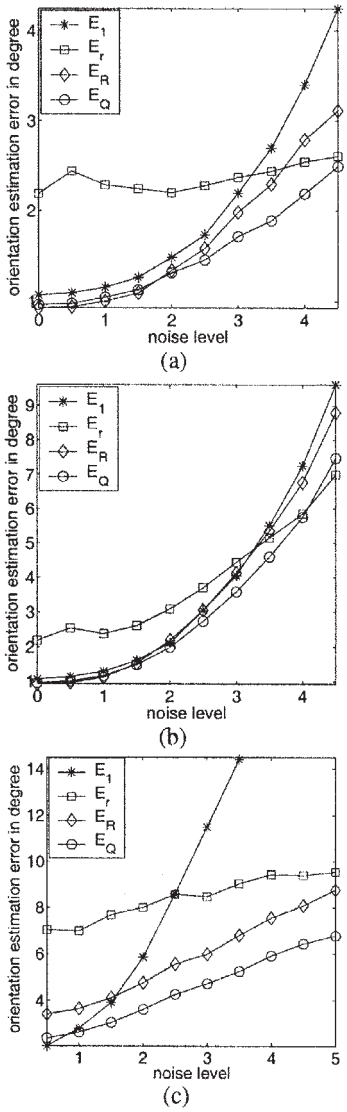

Fig. 7. Average absolute errors of orientation estimation against the noise level T, where E_1, E_r, E_R, and E_Q are errors of Θ_1^Γ, Θ_r^Γ, $\Theta_{R\Lambda}^\Gamma$, and $\Theta_{Q\Lambda}^\Gamma$, respectively. (a) 10% and (b) 50% pixels are corrupted by additive noise, and (c) an exclusive noise stroke crosses each estimation region Γ.

The gradient modulus normalization needs N additions and divisions. The introduced block-wise modulus normalization (17) needs $2M$ additions, $3M$ multiplications, and M square-root operations and divisions. The proposed approach of setting the orientation vector modulus to be its anisotropy estimate, however, needs only M additions and divisions. The computational consumption of the proposed estimates $\Theta_{Q\Lambda}^\Gamma$ and $Q_{Q\Lambda}^\Gamma$ is, although slightly higher than that of Θ_1^Γ and Q_1^Γ, lower than that of Θ_r^Γ and Q_r^Γ as well as $\Theta_{R\Lambda}^\Gamma$ and $Q_{R\Lambda}^\Gamma$. The computational efficiency of the proposed estimates $\Theta_{Q\Lambda}^\Gamma$ and $Q_{Q\Lambda}^\Gamma$ is advantageous to the online fingerprint authentication systems.

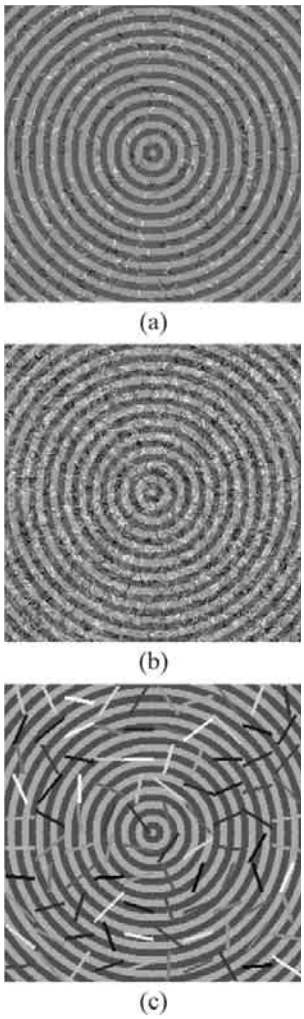

Fig. 8. Sample test images with $T = 3$ used for Fig. 7(a)–(c), respectively.

For the oriented patterns in Fig. 2(a) and (b), the proposed method results in $\Theta^{\Gamma}_{Q\Lambda} = 0^{\circ}$ and $\Theta^{\Gamma}_{Q\Lambda} = 0.8809^{\circ}$, respectively. The estimation error for Fig. 2(b) is, although slightly larger than that of Θ^{Γ}_{r} (0.7690°), significantly smaller than that of Θ^{Γ}_{1} (13.4574°). The anisotropy estimate $Q^{\Gamma}_{Q\Lambda}$ for Fig. 2(b) (0.8164) is smaller than that (0.8521) for Fig. 2(a), compared with Q^{Γ}_{1} values of 0.9139/0.8501 for Fig. 2(a) and (b). For the noise-free pattern in Fig. 3, the proposed $\Theta^{\Gamma}_{Q\Lambda}$ has a bias of 0.9646°, compared with 1.0714° and 2.1871° of Θ^{Γ}_{1} and Θ^{Γ}_{r}, respectively. For images in Fig. 3(a), $\Theta^{\Gamma}_{Q\Lambda}$ achieves the average absolute error of 1.3085°, compared with 1.4023° and 2.2521° of Θ^{Γ}_{1} and Θ^{Γ}_{r}, respectively. For images in Fig. 3(b), the error of $\Theta^{\Gamma}_{Q\Lambda}$ is 2.4980°, compared with 3.3551° and 2.7686° of Θ^{Γ}_{1} and Θ^{Γ}_{r}, respectively. The anisotropy estimates $Q^{\Gamma}_{Q\Lambda}$ for Fig. 3(a) and (b) are 0.7590 and 0.5764, respectively, compared with the corresponding Q^{Γ}_{r} values of 0.5155 and 0.4596. For Fig. 4(a) and (b), $Q^{\Gamma}_{Q\Lambda}$ is 0.8526 and 0.1036, respectively, compared with the corresponding Q^{Γ}_{1} values of 0.1117 and 0.8643. In addition, we noticed that the introduced $\Theta^{\Gamma}_{R\Lambda}$ has higher errors than the proposed $\Theta^{\Gamma}_{Q\Lambda}$ with 1.3897° and 3.2200° for Fig. 3(a) and (b), respectively.

It is worth noting that the proposed orientation estimation achieves smaller error than the both Θ^{Γ}_{1} and Θ^{Γ}_{r} for both

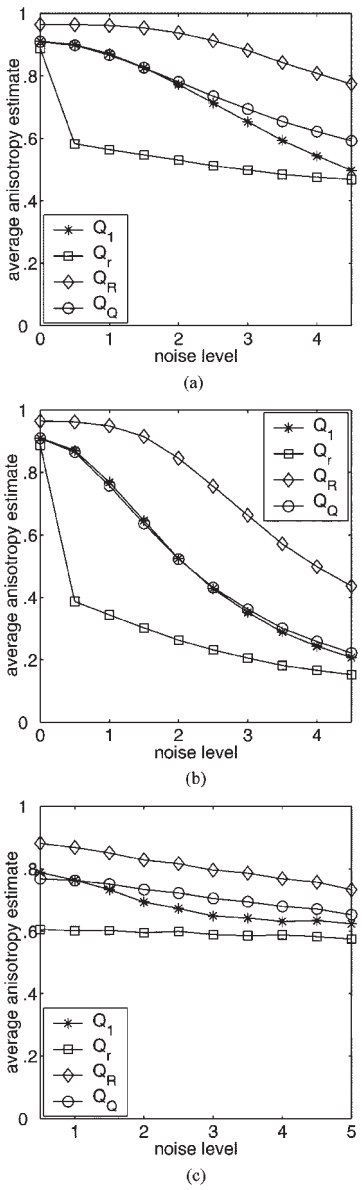

Fig. 9. Average anisotropy estimates against the noise level T of images used for Fig. 7(a)–(c), respectively, where Q_1, Q_r, Q_R, and Q_Q in the legend are short forms of Q^{Γ}_{1}, Q^{Γ}_{r}, $Q^{\Gamma}_{R\Lambda}$, and $Q^{\Gamma}_{Q\Lambda}$, respectively.

Fig. 3(a) and (b), as well as the noise-free pattern in Fig. 3. This is not a surprise because the proposed framework does not amplify weak noise (in the first stage of average) and suppresses not only the strong (in amplitude) noise but the dense (in occurrence) noise (in the second stage of average) as well. Furthermore, this new method does not lose the orientation inconsistency of gradients within the block (setting the modulus to be the anisotropy estimate instead of unity). It should be emphasized that the proposed orientation estimate $\Theta^{\Gamma}_{Q\Lambda}$ is not a simple compromise between the estimates Θ^{Γ}_{1} and Θ^{Γ}_{r}. Extensive experiments will demonstrate that further.

IV. Experimental Evaluation and Comparison

In this section, we employ both synthetic images and real fingerprints to test the accuracy and noise robustness of the concerned orientation estimation approaches. In all experiments,

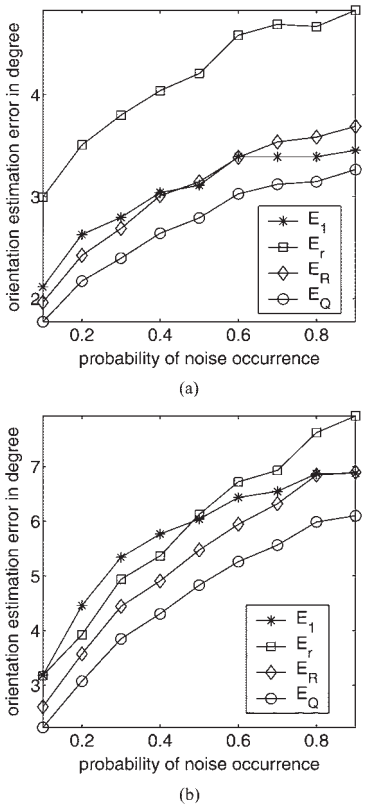

Fig. 10. Average absolute errors of orientation estimation against the noise occurrence probability, where E_1, E_r, E_R, and E_Q are errors of $\Theta_1^\Gamma, \Theta_r^\Gamma, \Theta_{R\Lambda}^\Gamma$, and $\Theta_{Q\Lambda}^\Gamma$, respectively. (a) $T = 2$. (b) $T = 3$.

the sizes of the estimation region Γ and block Λ^k are 25×25 and 5×5, respectively.

A. Testing With Synthetic Images

We synthesize the noise-oriented pattern as

$$f(t) = \begin{cases} s(t), & \text{with probability } q \\ s(t) + n(t), & \text{with probability } p - p' \\ m(t) + n(t), & \text{with probability } p' \end{cases} \tag{26}$$

with $p + q = 1$ and $p' \leq p$. $n(t)$ is additive noise and $m(t)$ exclusive noise. We simulate the additive oriented noise $n(t)$ by short lines (5 pixels in length and 1 pixel in width) with random orientations. For oriented exclusive noise $m(t)$, we use lines of three pixels in width crossing over at least one estimation region Γ with random orientations. This stroke noise appears often in real fingerprints. Alternate circle ridges and valleys of width 6 with gray levels of -1 and 1, respectively, are used to construct the oriented pattern. The constructed oriented pattern has size of 252×252 so that for each image, 100 local dominant orientations are estimated with nonoverlapping estimation regions. The average absolute estimation error is computed over all estimation regions of 20 images with independent noise. We test orientation estimates Θ_1^Γ, Θ_r^Γ, $\Theta_{R\Lambda}^\Gamma$, and $\Theta_{Q\Lambda}^\Gamma$, as well as the anisotropy estimates Q_1^Γ, Q_r^Γ, $Q_{R\Lambda}^\Gamma$, and $Q_{Q\Lambda}^\Gamma$.

By setting $p' = 0$, images are only corrupted by additive noise $n(t)$. Noise gray level is evenly distributed in $[-T, T]$. Fig. 7(a) and (b) illustrates the average absolute errors of orientation estimation against T with $p = 0.1$ and $p = 0.5$, respectively. They show that except for the case of $p = 0.5$ & $T > 4$, the proposed orientation estimate $\Theta_{Q\Lambda}^\Gamma$ outperforms the both conventional estimates Θ_1^Γ and Θ_r^Γ, where $\Theta_{Q\Lambda}^\Gamma$ significantly outperforms Θ_r^Γ for lower noise level and significant outperforms Θ_1^Γ for higher noise level. We also see that the introduced $\Theta_{R\Lambda}^\Gamma$ has about the same error as that of $\Theta_{Q\Lambda}^\Gamma$ for a low noise level, but its error increases as sharply as that of Θ_1^Γ with the increase of T. Fig. 8(a) and (b) shows two sample images with $T = 3$: one for $p = 0.1$ and the other for $p = 0.5$.

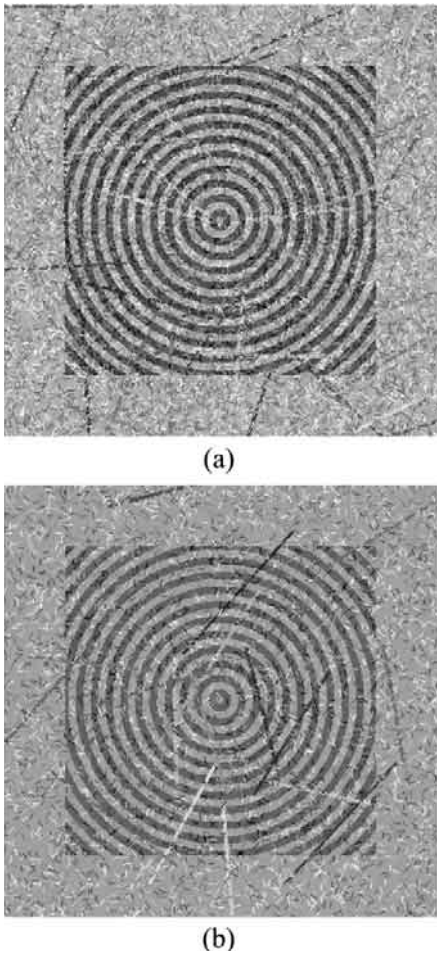

Fig. 11. Sample test images used for Fig. 10(a) with $p = 0.7$ and Fig. 10(b) with $p = 0.3$, respectively.

By setting $p = p'$ and $n(t) = 0$, images are only corrupted by exclusive noise $m(t)$. The noise gray level is evenly distributed in $[-T, T]$. Each estimation region Γ has one and only one noise stroke crossing the region. The noise occurrence probability is 0.12. A sample image with $T = 3$ is shown in Fig. 8(c). The average absolute errors of the orientation estimation against T are illustrated in Fig. 7(c). We see that the proposed $\Theta_{Q\Lambda}^\Gamma$ significantly outperforms all other estimates, except for $T = 0.5$, where Θ_1^Γ is slightly better than $\Theta_{Q\Lambda}^\Gamma$. The introduced $\Theta_{R\Lambda}^\Gamma$ performs better than Θ_r^Γ for all T values and better than Θ_1^Γ for $T > 1.5$. Fig. 7 also clearly shows the pros and cons of gradient normalization versus linear average.

Fig. 9(a)–(c) illustrates the average anisotropy estimates against T with noise conditions that are the same as those in Fig. 7(a)–(c), respectively. While all anisotropy estimates monotonously decrease with the increase of the noise level,

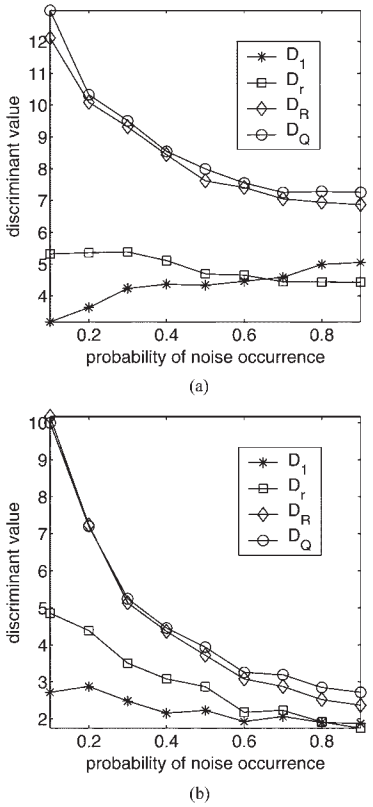

Fig. 12. Average discriminant values against the noise occurrence probability, where D_1, D_r, D_R, and D_Q in the legend are short forms of $\mathcal{D}_1^\Gamma$, $\mathcal{D}_r^\Gamma$, $\mathcal{D}_{R\Lambda}^\Gamma$, and $\mathcal{D}_{Q\Lambda}^\Gamma$, respectively. (a) $T = 2$. (b) $T = 3$.

Q_r^Γ is always lower, and $Q_{R\Lambda}^\Gamma$ is always higher than Q_1^Γ and $Q_{Q\Lambda}^\Gamma$. From Fig. 9, $Q_{Q\Lambda}^\Gamma$ and Q_1^Γ show a higher sensitivity to noise levels than Q_r^Γ and $Q_{R\Lambda}^\Gamma$. Although Q_1^Γ performs well for the constant contrast of the "signal" pattern, its problems were shown in Figs. 2 and 4 in the previous section.

Another test image of size 352×352 consists of an oriented pattern $\mathcal{O}$ in Fig. 8 of size 252×252 as foreground, located in the center of the image and the background $\mathcal{B}$ with a constant gray level of 1. Noise stroke $m(t)$ with length of 101 is injected into the image. Then, noise $n(t)$ is added to the image. Gray levels of both kinds of noise are evenly distributed in $[-T, T]$. The stroke occurrence probability is fixed as $p' = 0.1p$. Fig. 10(a) and (b) illustrates the average absolute errors of the foreground orientation estimates against p with $T = 2$ and $T = 3$, respectively. Fig. 10(a) and (b) demonstrates that the proposed orientation estimation approach significantly outperforms other approaches. Fig. 11(a) and (b) shows two sample images: one for $T = 2 \,\&\, p = 0.7$ and the other for $T = 3 \,\&\, p = 0.3$.

One of the important applications of the anisotropy estimate is the segmentation of the image into the oriented pattern and the background. The capability of discriminating between oriented and noise patterns is therefore a good indicator of how good an anisotropy estimate is. We define the discriminant as

$$\mathcal{D}_x^\Gamma = \frac{\left[\mathcal{M}\left(Q_x^\Gamma \,|\Gamma \in \mathcal{O}\right) - \mathcal{M}(Q_x^\Gamma \,|\Gamma \in \mathcal{B})\right]^2}{\mathcal{V}(Q_x^\Gamma \,|\Gamma \in \mathcal{O}) + \mathcal{V}(Q_x^\Gamma \,|\Gamma \in \mathcal{B})} \tag{27}$$

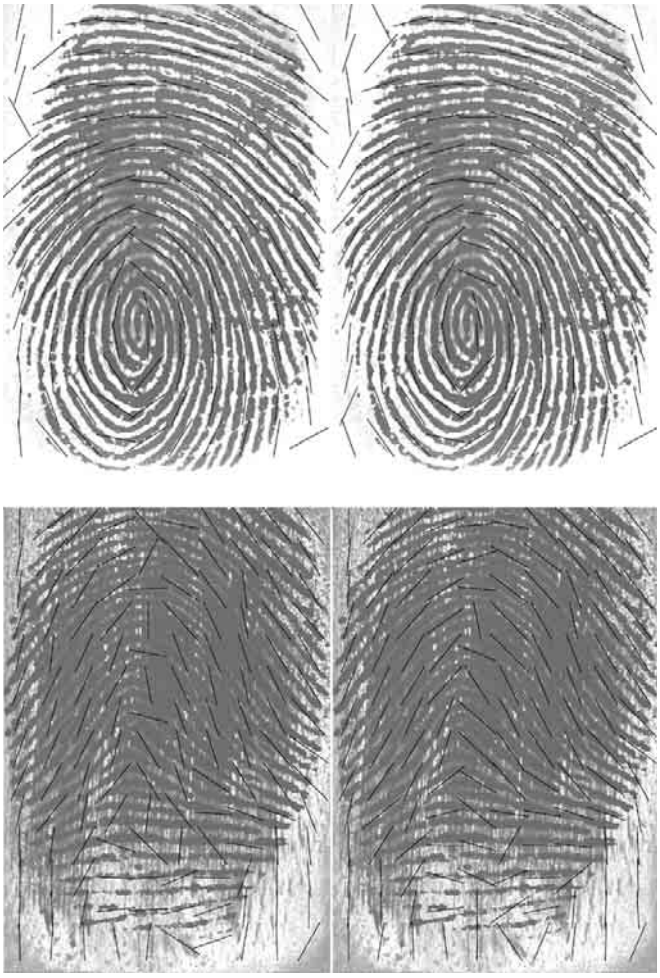

Fig. 13. Two real fingerprints and orientation fields, where the left and right parts show Θ_1^Γ and $\Theta_{Q\Lambda}^\Gamma$, respectively.

Fig. 14. Two real fingerprints and orientation estimates where visible difference can be found. Unmarked lines and lines marked by circles and dots represent $\Theta_{Q\Lambda}^\Gamma$, Θ_1^Γ, and Θ_r^Γ, respectively.

where $\mathcal{M}(\cdot)$ and $\mathcal{V}(\cdot)$ are the mean and variance operators, respectively. The employed estimation method is indicated by x. $\Gamma \in \mathcal{O}$ if Γ has more pixels of the oriented pattern than those of the background. Otherwise, $\Gamma \in \mathcal{B}$. Fig. 12(a) and (b) illustrates the average discriminants against p of images used for

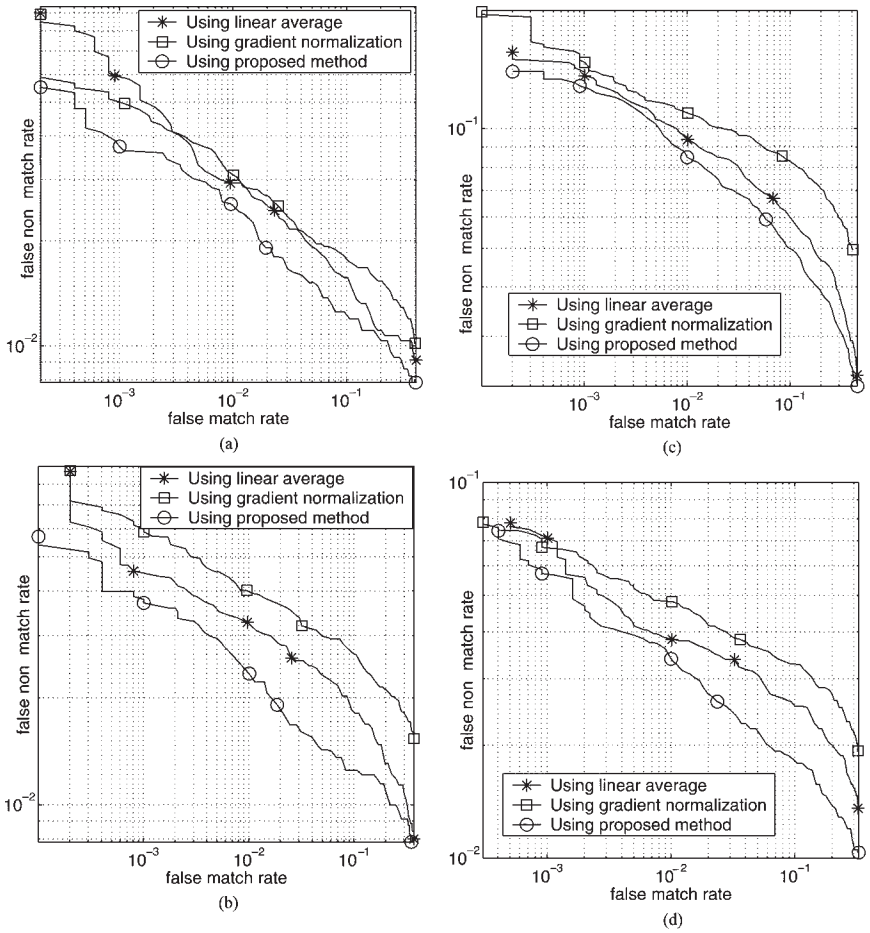

Fig. 15. ROC curves of fingerprint verification algorithms using different orientation and anisotropy estimates for databases (a) Db1_a, (b) Db2_a, (c) Db3_a, and (d) Db2_a*. Equal errors FMR = 0.01, 0.001, and the curve endings are marked by $*$, $\square$, and $\circ$, respectively, for the linear, gradient normalizing, and proposed methods.

Fig. 10(a) and (b), respectively. They demonstrate that the proposed anisotropy estimate $Q^{\Gamma}_{Q\Lambda}$ is much better in discriminating the oriented pattern from the noise pattern than the conventional estimates Q^{Γ}_{1} and Q^{Γ}_{r}.

B. Testing With Sample Real Fingerprints

It is difficult to measure the estimation accuracy quantitatively for real fingerprints. We plot the orientation estimates by oriented lines and superimpose them on the real fingerprint. In this way, some large orientation estimation errors can be visible. Fig. 13 shows good (top) and bad (bottom) fingerprints and the orientation estimates Θ^{Γ}_{1} (left) and $\Theta^{\Gamma}_{Q\Lambda}$ (right).

For the good fingerprint, $\Theta^{\Gamma}_{Q\Lambda}$ is better than Θ^{Γ}_{1} in the high curvature area above the core point. The "signal" orientation in the estimation region is not constant in the high curvature area. The desired orientation estimate in this case is usually the mean of the gradient orientations rather than the mean of the gradient vectors. Therefore, the proposed method usually performs better than the linear average method in the high curvature area. If the estimation concern is only to catch the mean of the orientation distribution, the gradient normalization should be slightly better than the proposed method. This was shown by the orientation estimates of $\Theta^{\Gamma}_{Q\Lambda} = 0.8809°$, $\Theta^{\Gamma}_{r} = 0.7690°$, and $\Theta^{\Gamma}_{1} = 13.4574°$ for Fig. 2(b). For the bad fingerprint, we can see a large number of orientation estimates $\Theta^{\Gamma}_{Q\Lambda}$ visibly better than Θ^{Γ}_{1}. There are a small number of blocks where $\Theta^{\Gamma}_{Q\Lambda}$ is inferior to Θ^{Γ}_{1}. This is because noise, although small in amplitude, densely occurs, whereas the ridge-valley structure, although strong in amplitude, sparsely appears so that noise is not well suppressed by the linear smoothing step of the proposed method in the small blocks Λ_k. The problem can be solved by increasing the size of Λ_k. Fig. 14 shows another two fingerprints, where $\Theta^{\Gamma}_{Q\Lambda}$ (unmarked lines) and Θ^{Γ}_{1} (lines marked by circles) are plotted if and only if $\left|\Theta^{\Gamma}_{Q\Lambda} - \Theta^{\Gamma}_{1}\right| > 11.25°$, and $\Theta^{\Gamma}_{Q\Lambda}$ and Θ^{Γ}_{r} (lines marked by dots) are plotted if and only if $\left|\Theta^{\Gamma}_{Q\Lambda} - \Theta^{\Gamma}_{r}\right| > 11.25°$. Fig. 14 demonstrates that the proposed orientation estimate $\Theta^{\Gamma}_{Q\Lambda}$ is visibly more robust to low-quality fingerprints than the two conventional estimates Θ^{Γ}_{1} and Θ^{Γ}_{r}.

C. Verification Testing With Large Real Fingerprint Database

The local dominant orientation is a crucial parameter for fingerprint verification algorithms. The verification performance on the large database will objectively reflect the robustness of the orientation estimation. The verification algorithm [4], [28] is used in the testing, which consists of two parts, i.e., minutia extraction and minutia matching. Four fingerprint databases [29], [30] containing 3200 real fingerprints are used in the experiment, two of which (FVC2002 Db1_a and Db2_a) were

TABLE I
EQUAL ERRORS OF VARIOUS METHODS AND DATABASES/AVERAGE ENROLL TIME IN MILLISECONDS FOR Db1_a

method	Db1_a	Db2_a	Db3_a	Db2_a*
linear	2.39/31.3	2.57	6.78	3.32
normalization	2.52/33.8	3.19	8.46	3.72
proposed	1.93/31.5	1.89	5.88	2.49

captured by optical sensors, and the other two (FVC2002 Db3_a and FVC2000 Db2_a, denoted by Db2_a*), were captured by capacitive sensors. The performance evaluation procedure of FVC2002 is adopted. However, unlike FVC2002, which allows a database-specific configuration file, the algorithm is not optimized for specific database. Orientation is estimated every 5 pixels along x- and y-coordinates with a fixed window size of 25×25. We integrate the estimates Θ_1^Γ, Q_1^Γ, Θ_r^Γ, Q_r^Γ, and $\Theta_{Q\Lambda}^\Gamma$, $Q_{Q\Lambda}^\Gamma$ into the algorithm and test the respective fingerprint verification performances with the four databases. The algorithm was executed under Windows XP Professional O.S. on a HP xw4100 (Intel Pentium 4 at 3.0 GHz) PC.

Fig. 15 shows the receiver operating curves, and Table I records the equal errors for the various methods and databases and the average enroll time for Db1_a. The average matching time of all methods is 0.62 ms for Db1_a. The enroll and verification use the same minutia extraction algorithm so that the verification time is the enroll time plus matching time. We see that the proposed method increases the verification time by only 0.6%, whereas the gradient normalization is increased by 7.8% from that with the linear average (31.92 ms). There is therefore no problem in applying the proposed method in an online fast fingerprint verification system. Fig. 15 and Table I demonstrate that the proposed orientation estimation method consistently improves the fingerprint verification accuracy for all operating points, although the improvement at some points is small. As the employed verification algorithm is a very fast algorithm that only uses minutiae in the matching, the verification error caused by the extremely small number of minutiae in the common area of the template and input fingerprints, which is the major part of the verification error for the four FVC databases based on our observation, cannot be reduced by the proposed orientation estimation method. In addition, some problems caused by heavy noise in a large area cannot be well solved by the proposed method with a predetermined smoothing window size. Some recursive orientation regularization frameworks with adaptively enlarged window size [8], [10] can be incorporated to solve such problems. However, using an anisotropy estimate to determine the window size may worsen the orientation estimation in the high curvature area, which, similar to the noisy area, also reduces the anisotropy. Therefore, we do not implement the recursive orientation regularization approach in the fingerprint verification algorithm before finding an effective way to determine the adaptive smoothing window size.

V. CONCLUSION

Fingerprint local orientation estimation is a crucial step for the whole recognition system. This paper analyzes the noise robustness of the gradient-based orientation estimation methods that are widely used in the fingerprint authentication system. The characteristics of the corresponding anisotropy estimates are studied as well. It shows that the gradient modulus normalization has both advantages and disadvantages. Its pros and cons in the orientation and anisotropy estimation are presented. A two-stage averaging framework with block-wise modulus handling of the orientation vector is introduced to inherit the merits of the both linear and normalized vector averaging. We further propose to set the modulus of an orientation vector to be its anisotropy estimate instead of unity so that the orientation inconsistency of gradients is included in the second stage of averaging. These two measures improve the noise robustness of the fingerprint local dominant orientation estimation. Furthermore, the proposed approach leads to an improved anisotropy estimate that reflects the characteristics of the fingerprint more effectively. In addition, the approach requires fewer computation operations than the gradient modulus normalization and even less than the block-wise modulus normalization. This gives the advantage to the online application of a fingerprint authentication system. Extensive experiments using both synthetic images and real fingerprints verify the feasibility of the proposed approach and demonstrate its robustness to noise and low-quality fingerprints. It outperforms the conventional linear and normalized averaging methods as well as the block-wise modulus normalization approach. The developed technique improves the robustness of a fingerprint authentication system to low-quality fingerprints, which is crucial for the system's massive application, such as securing multimedia.

REFERENCES

[1] U. Uludag and A. K. Jain, "Multimedia content protection via biometrics-based encryption," in *Proc. Int. Conf. Multimedia Expo*, Baltimore, MD, Jul. 2003.

[2] D. Maltoni, D. Maio, A. K. Jain, and A. Prabhakar, *Handbook of Fingerprint Recognition*. New York: Springer, 2003.

[3] L. Hong, Y. Wan, and A. K. Jain, "Fingerprint image enhancement: Algorithm and performance evaluation," *IEEE Trans. Pattern Anal. Machine Intell.*, vol. 20, no. 8, pp. 777–789, Aug. 1998.

[4] X. D. Jiang, W. Yau, and W. Ser, "Detecting the fingerprint minutiae by adaptive tracing the gray level ridge," *Pattern Recogn.*, vol. 34, no. 5, pp. 999–1013, May 2001.

[5] D. Maio and D. Maltoni, "Direct gray-scale minutiae detection in fingerprints," *IEEE Trans. Pattern Anal. Machine Intell.*, vol. 19, no. 1, pp. 27–39, Jan. 1997.

[6] A. K. Jain, S. Prabhakar, and L. Hong, "A multichannel approach to fingerprint classification," *IEEE Trans. Pattern Anal. Machine Intell.*, vol. 21, no. 4, pp. 348–359, Apr. 1999.

[7] R. Cappelli, A. Lumini, D. Maio, and D. Maltoni, "Fingerprint classification by directional image partitioning," *IEEE Trans. Pattern Anal. Machine Intell.*, vol. 21, no. 5, pp. 402–421, May 1999.

[8] A. K. Jain, L. Hong, and R. Bolle, "On-line fingerprint verification," *IEEE Trans. Pattern Anal. Machine Intell.*, vol. 19, no. 4, pp. 302–314, Apr. 1997.

[9] A. Almansa and T. Linderberg, "Fingerprint enhancement by shape adaptation of scale-space operators with automatic scale selection," *IEEE Trans. Image Process.*, vol. 9, no. 12, pp. 2027–2042, Dec. 2000.

[10] A. K. Jain, L. Hong, S. Pankanti, and R. Bolle, "An identity-authentication system using fingerprints," *Proc. IEEE*, vol. 85, no. 9, pp. 1365–1388, Sep. 1997.

[11] A. M. Bazen and S. H. Gerez, "Segmentation of fingerprint images," in *Proc. 12th Annu. Workshop Circuits, Syst. Signal Process.*, Nov. 2001.

[12] E. Lim, X. D. Jiang, and W. Yau, "Fingerprint quality and validity analysis," in *Proc. IEEE Int. Conf. Image Process.*, vol. 1, Rochester, NY, Sep. 2002, pp. 469–472.

[13] M. Kass and A. Witkin, "Analyzing oriented patterns," *Comput. Vision, Graphics, Image Process.*, vol. 37, no. 3, pp. 362–385, 1987.

[14] M. J. Donahue and S. I. Rokhlin, "On the use of level curves in image analysis," *Image Understanding*, vol. 57, no. 2, pp. 185–203, 1993.
[15] O. A. Zuniga and R. M. Haralick, "Integrated directional derivative gradient operator," *IEEE Trans. Syst., Man, Cybern.*, vol. SMC-17, no. 3, pp. 508–517, Mar. 1987.
[16] J. A. Noble, "Finding corners," *Image Vision Comput.*, vol. 6, pp. 121–128, 1988.
[17] S. Ando, "Image field categorization and edge/corner detection from gradient covariance," *IEEE Trans. Pattern Anal. Machine Intell.*, vol. 22, no. 2, pp. 179–190, Feb. 2000.
[18] A. R. Rao and R. C. Jain, "Computerized flow field analysis: Oriented texture fields," *IEEE Trans. Pattern Anal. Machine Intell.*, vol. 14, no. 7, pp. 693–709, Jul. 1992.
[19] A. R. Rao and B. G. Schunk, "Computing oriented texture fields," *CVGIP: Graphical Models Image Process.*, vol. 53, pp. 157–185, 1991.
[20] J. Biguen, G. H. Granlund, and J. Wiklund, "Multidimensional orientation estimation with applications to texture analysis and optical flow," *IEEE Trans. Pattern Anal. Machine Intell.*, vol. 13, no. 8, pp. 775–789, Aug. 1991.
[21] A. R. Rao, *A Taxonomy for Texture Description and Identification*. New York: Springer-Verlag, 1990.
[22] N. K. Ratha, S. Y. Chen, and A. K. Jain, "Adaptive flow orientation-based feature extraction in fingerprint images," *Pattern Recogn.*, vol. 28, no. 11, pp. 1657–1672, Nov. 1995.
[23] A. M. Bazen and S. H. Gerez, "Systematic methods for the computation of the directional fields and singular points of fingerprints," *IEEE Trans. Pattern Anal. Machine Intell.*, vol. 24, no. 7, pp. 905–919, Jul. 2002.
[24] A. K. Jain, S. Prabhakar, and L. Hong, "Filterbank-based fingerprint matching," *IEEE Trans. Image Process.*, vol. 9, no. 5, pp. 846–859, May 2000.
[25] P. Perona, "Orientation diffusions," *IEEE Trans. Image Process.*, vol. 7, no. 3, pp. 457–467, Mar. 1998.
[26] P. H. Gregson, "Using angular dispersion of gradient direction for detecting edge ribbons," *IEEE Trans. Pattern Anal. Machine Intell.*, vol. 15, no. 7, pp. 682–696, Jul. 1993.
[27] D. Maio and D. Maltoni, "Ridge-line density estimation in digital images," in *Proc. 14th Int. Conf. Pattern Recogn.*, vol. 1, Brisbane, Australia, Aug. 1998, pp. 534–538.
[28] X. D. Jiang and W. Yau, "Fingerprint minutiae matching based on the local and global structures," in *Proc. 15th Int. Conf. Pattern Recogn.*, vol. 2, Barcelona, Spain, Sep. 2000, pp. 1042–1045.
[29] D. Maio, D. Maltoni, R. Cappelli, J. L. Wayman, and A. K. Jain, "FVC2000, fingerprint verification competition," *IEEE Trans. Pattern Anal. Machine Intell.*, vol. 24, no. 3, pp. 402–412, Mar. 2002.
[30] ——, "FVC2002, second fingerprint verification competition," in *Proc. 16th Int. Conf. Pattern Recogn.*, vol. 3, Quebec City, QC, Canada, Aug. 2002, pp. 811–814.

Xudong Jiang (M'02) received the B.Eng. and M.Eng. degrees from the University of Electronic Science and Technology of China, Chengdu, China, in 1983 and 1986, respectively, and the Ph.D. degree from the University of German Federal Armed Forces, Hamburg, Germany, in 1997, all in electrical and electronic engineering.

From 1986 to 1993, he was a Lecturer at the University of Electronic Science and Technology of China. From 1993 to 1997, he was with the University of German Federal Armed Forces as a scientific assistant. From 1998 to 2002, he was with the Centre for Signal Processing, Nanyang Technological University, Singapore, first as a Research Fellow and then as a Senior Research Fellow, where he developed a fingerprint verification algorithm that achieved the fastest and the second most accurate fingerprint verification in the International Fingerprint Verification Competition (FVC2000). From 2002 to 2004, he was a Lead Scientist and Head of the Biometrics Laboratory, Institute for Infocomm Research, Singapore. Currently, he is an Assistant Professor with the School of Electrical and Electronic Engineering, Nanyang Technological University. His research interests include pattern recognition, neural networks, image processing, computer vision, biometrics, adaptive signal processing, and spectral analysis.

Dr. Jiang received two Science and Technology Awards from the Ministry for Electronic Industry of China and was a recipient of the German Konrad–Adenauer Foundation Young Scientist Scholarship.